On the evolution of large ultramafic magma chambers and timescales for flood basalt eruptions

Leif Karlstrom[1] and Mark Richards[1]

Received 13 December 2010; revised 23 May 2011; accepted 6 June 2011; published 27 August 2011.

[1] Large igneous provinces are characterized by magmatic activity on two distinct timescales. While these provinces have total active lifetimes of order 10–30 Ma, most of the erupted volume is emplaced within 1 Ma in many cases. The longer timescale is consistent with plume or tectonic models for mantle melting responsible for flood volcanism, but the shorter "main stage" timescale is enigmatic. We hypothesize that cessation of main stage eruptions reflects shutoff of dike propagation from the deep crust due to the onset of thermally activated creep on a ~1 Ma timescale, with intrusive processes and minor eruptions continuing over 10–30 Ma. To test this hypothesis we model deep magma differentiation and the stability of Moho level magma reservoirs. Assuming mantle volatile contents, fractionation results in concentration and deep exsolution of CO_2, with the geothermal gradient and melt influx setting the timescale for buoyancy production and thus timing between individual eruptions. Chemical evolution generally occurs rapidly compared to heat conduction from the magma body. Although the viscous response of surrounding rocks depends on lower crustal rheology, we find that thermally induced creep can reasonably prevent dike propagation within 1 Ma of intrusion. However, if melt influx is high or heat transfer from the magma chamber is low, viscous creep may outpace differentiation. In this regime, continued melt influx spreads along the Moho until external stresses provide a destabilizing trigger. The coevolution of large-scale melting and lower crustal rheology may thus control a progression of large igneous province emplacement from largely eruptive to largely intrusive magmatism.

Citation: Karlstrom, L., and M. Richards (2011), On the evolution of large ultramafic magma chambers and timescales for flood basalt eruptions, *J. Geophys. Res.*, *116*, B08216, doi:10.1029/2010JB008159.

1. Introduction

[2] The emplacement of large igneous provinces (LIPs) is a poorly understood process. Endogenous hypotheses for the large eruptive volumes associated with LIPs include mantle plume heads, or starting plumes, impinging upon the lithosphere [e.g., *Morgan*, 1971; *Richards et al*., 1989; *Campbell and Griffiths*, 1990], asthenospheric convection [e.g., *King and Anderson*, 1995] and lithospheric delamination [e.g., *Tanton and Hager*, 2000; *Hales et al*., 2005], suggesting source regions for these events at a range of depths. Exogenic origins for LIPs have also been proposed [e.g., *Jones et al*., 2002]. Most existing endogenous models for the genesis of flood basalt provinces do not explain the geologically short durations (1 Ma or less) of the "main stage" eruptions that usually account for most of the erupted basalt volumes for LIPs [*Courtillot and Renne*, 2003].

[3] Other important aspects of LIPs awaiting satisfactory explanation include the magnitude of coevolving dynamic topography, the common (although not exclusive) association of LIPs with continental rifting events, and the remarkably uniform compositions of the main stage basalts. There seems to be little consensus regarding the nature of magma chambers that appear necessary to fractionate and homogenize the large quantities of basaltic melt before eruption, despite the existence of extensive seismic evidence for large volumes of deep ultramafic intrusive/cumulate bodies underlying LIPs [*Cox*, 1980; *Ridley and Richards*, 2010], and extensive sills at more shallow depths [*Elliot and Fleming*, 2008]. These problems may be largely attributed to our lack of understanding of what happens to the primary melts produced in the mantle as they rise and interact with the overlying lithosphere and crust.

[4] In our view there are a number of important questions related to the plumbing of LIP magmatism. What are the melt production rates predicted by the various LIP generation hypotheses, and how might this melt accumulate in chambers? At what depths would these magma bodies form, and what factors govern their emplacement? Are there multiple stages or depths of fractionation and melt storage in the crust?

[5] Other open questions are more directly linked to the geologic record: Why are the main stage eruptions so brief and so uniform in individual flow characteristics (erupted volumes, major and trace element compositions)? How do inflation and deflation of intrusions affect uplift and subsidence at the surface? To what extent can exposed large

[1]Department of Earth and Planetary Science, University of California, Berkeley, California, USA.

0148-0227/11/2010JB008159

intracrustal mafic intrusions, and continental diking events be related to the eruption of flood basalts?

[6] Of these questions, we are particularly drawn to that of the remarkably short duration of the main stage eruptions of flood basalts. The largest volumes of basalts are erupted within ~0.5 – 1.0 Ma, but primary mantle melting events during LIPs are expected to be of duration >10 Ma [e.g., *Farnetani and Richards*, 1994; *Leitch and Davies*, 2001]. Could primary melt be ponded in deep sills or magma chambers for an extended period before eruptions occur? This seems highly unlikely as such long-term storage is known not to occur in the oceanic lithosphere and crust beneath modern hot spots [*Hauri et al*., 1996]. A more attractive hypothesis is that large-scale eruptions are controlled by the ability of the overlying crust to propagate fractures (dikes) to feed eruptions, limited by the onset of viscous flow as the crust surrounding the magma body heats up in time [*Jellinek and DePaolo*, 2003; *de Silva and Gosnold*, 2007].

[7] We explore the latter hypothesis first by summarizing several independent lines of evidence that connect deep magmatic processes with eruptive processes in LIPs. We then formulate a model for the evolution of melt within and elastic deviatoric stresses surrounding a deep magma chamber. Finally, we apply these ideas to certain observational aspects of LIPs, thereby beginning to address the processes that occur between primary melting in the mantle and the eruption of flood basalts in both continental and oceanic settings.

2. The Observed Time Progression of LIP Magmatism

[8] From radiometric and magnetostratigraphic dating it appears that many flood basalt provinces have a similar time progression of eruptive style and cumulative output. Across the spectrum of Phanerozoic LIPs recognized so far, in nearly every case there is a punctuated early phase of flood basalt volcanism in which ~80 – 95% of the total volume of lavas are extruded [e.g., *Courtillot and Renne*, 2003], often an order of magnitude shorter than the total duration of the event, during which the style and composition of erupted lavas can vary greatly [*Jerram and Widdowson*, 2005]. This trend has been shown for, among others, the Columbia River Basalts [*Barry et al*., 2010], the Parana-Etendeka province [*Marzoli et al*., 1999], the North Atlantic province [*Storey et al*., 2007], and the Deccan traps [*Allegre et al*., 1999].

[9] Most LIPs are underlain by large mafic-ultramafic intrusive bodies, widely observed in the seismic record [*Ridley and Richards*, 2010]. This observation is not unexpected, in fact the existence of cumulate bodies may be predicted from the fact that sublithospheric melting of mantle plumes results in primary magmas of ultramafic, not basaltic, composition that are too dense to rise above the Moho or erupt [*Farnetani et al*., 1996]. Magma derived from 20% partial melting of a model pyrolite at 2 GPa results in a melt composition that includes 18% MgO and a corresponding melt density of about 2.9 kg/m^3 at Moho depths, more dense than the lowermost (gabbroic) oceanic crust. Thus we envision a three-stage process of (1) magma genesis in the mantle, (2) crystal fractionation (mainly olivine and pyroxene) at near-Moho depths in large sill complexes, and (3) eruption (or higher level intrusion) of basaltic magmas, as summarized in Figure 1. In fact, *Cox* [1980] inferred essentially the same sequence of events from largely petrological considerations.

[10] Explicit petrogenic models for the thickened crust of the Ontong-Java plateau, the largest LIP known [*Coffin and Eldholm*, 1994], show that the seismic velocity structure underlying the plateau can be explained in terms of sublithospheric mantle melting, deep fractionation, and ultimately eruption of residual basaltic magma [*Farnetani et al*., 1996]. These petrological models suggest that of order 2/3 the total melt volume is intruded material, with maximum crustal thicknesses reaching up to 40 km, and representing more than 30 km of crustal thickening relative to normal oceanic crust. Where high-quality seismic data are available beneath continental flood basalt provinces (Emeishan, Columbia River, Deccan, Siberia), high-velocity structures (Vp ~ 6.9–7.5 km/sec) are typically found immediately overlying the Moho in layers 5–15 km thick [*Ridley and Richards*, 2010]. Oceanic plateau LIPs exhibit similar high velocity layers. These structures are similar to inferred ultramafic underplating structures seen beneath active hot spots such as Hawaii, the Marquesas and others [e.g., *Watts and Brink*, 1989; *McNutt and Bonneville*, 2000; *Kopp et al*., 2003; *Contreras-Reyes et al*., 2010], suggesting that lower crustal ultramafic intrusive bodies are a common feature of hot spot magmatism. Radiometric dating of uplift markers also provides some evidence that intrusions may be, at least in part, responsible for the broad bathymetric swells around hot spot islands [*Ramalho et al*., 2010].

[11] Petrogenetic models for flood basalt volcanism based on hot plume material melting beneath mature lithosphere suggest that these deep seismic structures consist in large part of olivine and clinopyroxene cumulates [*Cox*, 1980; *Furlong and Fountain*, 1986; *Farnetani et al*., 1996]. Such fractionation is necessary to produce basalts with typical MgO contents of ~3 – 6%, as in the vast bulk of observed flood basalts, from primary melts with MgO of ~20% such as result from hot, deep melting beneath the lithosphere.

3. Posteruption Uplift and Doming

[12] The overall question of uplift and subsidence associated with LIPs is controversial, complicated by the nonunique transfer function linking mantle dynamics and surface topography. Traditional mantle plume head models predict up to several kilometers of precursory uplift, and similar postemplacement subsidence for LIPs [e.g., *Campbell and Griffiths*, 1990; *Farnetani and Richards*, 1994; *Saunders et al*., 2007]. Evidence for general large-amplitude uplift is present in some cases and lacking in others, however, and thermochemical plume models [*Farnetani and Samuel*, 2005; *Burov et al*., 2007] suggest that uplift associated with plume impingement on the lithosphere may be much more complex.

[13] Regardless of the melt generation mechanism, if the 10 Ma timescale for post main stage eruptions is accompanied by intrusion rather than eruptions, we would expect dynamic topography of similar duration. And there is geologic evidence for continued uplift long after the main stage flood basalt eruptions occur. *Ito and Clift* [1998] studied Deep Sea Drilling Project and Ocean Drilling Program data to constrain the uplift and subsidence histories of the three largest Pacific plateaus, Ontong-Java, Manihiki, and Shatsky Rise. In all

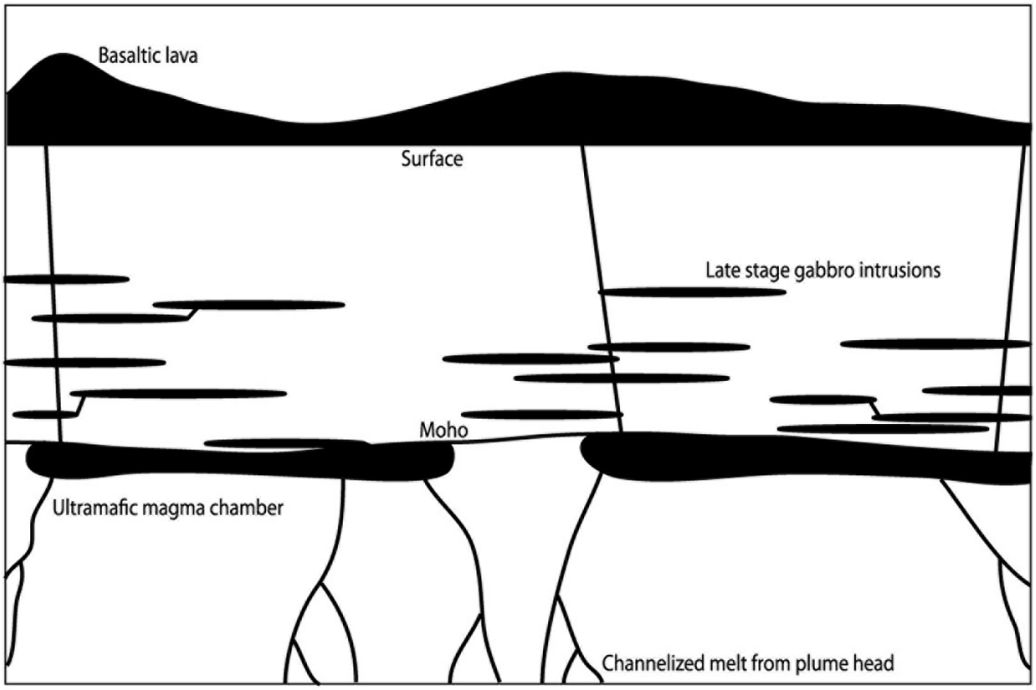

Figure 1. Conceptual model for LIP plumbing. Channelized melt from the upper mantle ponds at the base of the crust, forming large continuous magma reservoirs that differentiate to make basalts. These chambers inflate until destabilization occurs, erupting flood basalts on the surface and intruding gabbroic sills into higher crustal levels.

three cases, subsidence postdating the onset of eruptions is recorded by marine sedimentary sequences overlying the basaltic basement rocks. Similar histories are confirmed for the Ontong-Java plateau [*Roberge et al*., 2005] and the Kerguelen plateau [*Coffin and Eldholm*, 1994]. Notably, in all three cases studied by *Ito and Clift* [1998] there is a subsidence deficit: purely thermal models for plume generated magmatism predict postemplacement subsidence at least ~1 km more than observed. This deficit has been attributed to large volume intrusions that continue for 10–30 Ma following the initial short-lived outburst of basaltic eruptions [*Ito and Clift*, 1998; *Coffin and Eldholm*, 1994].

[14] LIP-related doming is also reported along the coast of southeastern Greenland in the Kangerdlugssuaq area [*Brooks*, 1973; *Nielsen and Brooks*, 1981; *Brooks*, 1982]. This region along the Denmark Strait was covered with up to 9 km of basalt at the onset of the North Atlantic Tertiary flood basalt event, with flows apparently accommodated by simultaneous subsidence as they were emplaced. Following these eruptions, and accompanying the opening of the North Atlantic basin, an area of horizontal dimension ~300 km along the Kangerdlugssuaq coastline experienced a broad domal uplift of amplitude at least 4 km, estimated to have occurred within 10 Ma of the flood basalt eruptions. Continued intrusion of ultramafic magmas into the deep crust [e.g., *White et al*., 2008] provides a plausible explanation for this doming. Indeed, abundant shallow crustal intrusive activity followed the basalt eruptions in this area, including the Skaergaard and other gabbroic intrusions shortly following the main extrusive episode, with more evolved syenitic intrusions 5 Ma later [*Tegner et al*., 2008].

[15] Finally, we note an additional observation from the Galapagos Archipelago that appears relevant to the question of deep intrusion. The Galapagos Islands are formed upon a broad platform of anomalously thick oceanic crust bounded on its SSW side by a steep escarpment of unknown origin. The SSW escarpment of the Galapagos Platform is now understood to be composed of many small topographic shelves that must predate the subsequent formation of the multiple shield complexes that have formed the islands and seamounts of the Galapagos Archipelago [*Geist et al*., 2005]. The crustal thickness of the platform approaches 14–15 km [*Feighner and Richards*, 1994], and modeling suggests that about one third of this material must be mafic-ultramafic bodies intruded as the oceanic lithosphere passed over the Galapagos mantle plume. We believe the Galapagos Platform and similar oceanic islands may also represent a case of massive igneous intrusion in the wake of initial basaltic eruption and shield formation.

4. Evolving Density of Primary Melt

[16] We are interested in what factors other than the timescale for mantle melting may control the timescale for flood basalt eruptions. Our modeling thus considers the end-member scenario in which extraction of partial melt from a plume head impinging upon the lithosphere occurs rapidly, generating a supply of magma that rises toward the base of the crust for the lifetime of decompression melting. This is assumed to be longer than the duration of main phase eruptions [e.g., *Farnetani and Richards*, 1994]. Assuming that individual main stage eruptions are controlled by rupture of a

single magma reservoir, there are two possibilities to consider. Failure may initiate internally from the chamber, as stresses accumulate through recharge and buoyancy evolution driving dikes to the surface. Alternatively, there may be some external trigger that destabilizes the chamber and drives dike propagation.

[17] Initial melting of a pyroxenite upper mantle will generate ultramafic magma that is more dense than the overlying crust, so that the density and rigidity contrast at the Moho will trap melt until it evolves sufficient buoyancy to erupt. This buoyancy is generated by a combination of fractional crystallization and progressive concentration of incompatible volatile species such as H_2O and CO_2 in the liquid. Depending on the depth and volatile concentration, and neglecting phase separation between bubbles and melt, exsolution of CO_2 may occur at Moho depths causing dramatically decreasing magma density and increasing compressibility. We explore these effects in numerical experiments combining the petrological modeling program pMELTS [*Ghiorso and Sack*, 1995; *Asimow and Ghiorso*, 1998; *Ghiorso et al.*, 2002] with a joint H_2O and CO_2 solubility model calibrated for ultramafic magmas [*Papale*, 1999]. We assume a mantle pyrolite at 2 GPa (~60 km depth), and raise the temperature about 200°C above the normal mantle adiabat, sufficient to cause 10% partial melting. Primary volatile contents are estimated based on solubility experiments at mantle temperatures and pressures, which suggest upper mantle water contents of ~0.1 wt% up to nearly 1 wt% and CO_2 contents of ~0.01 to ~0.1 wt% [*Dasgupta and Hirschmann*, 2006; *Smyth et al.*, 2006]. We do not attempt to explore this parameter range here, instead choosing a mantle concentration of 0.1 wt% H_2O and 0.05 wt % CO_2 to illustrate the effect of volatiles on melt evolution.

[18] The extraction and fractionation simulation then progresses as follows. Melt rises adiabatically to a pressure of either 300 MPa (~10 km depth) or 8 MPa (~30 km depth) to approximate a typical Moho depth in oceanic or continental settings. The melt at this stage is ultramafic, with 20% MgO, a density of 2.75–2.85 kg/m^3 (depending on depth and volatile content), and volatile contents of 0.5 wt% CO_2 and 1 wt% H_2O. These volatile contents are similar to Hawaiian lavas [*Gerlach et al.*, 2002], but might be underestimates for LIP events [*Lange*, 2002].

[19] We then simulate the storage and crystallization of this melt in a magma chamber. Cooling simulations are performed isochorically and isobarically, as end-member fractionation scenarios [*Fowler and Spera*, 2008]. Isochoric crystallization assumes a rigid container, letting pressure adjust to the volume changes induced by phase change. Isobaric crystallization instead fixes pressure, leaving the container volume to adjust freely. Either case is an idealization of crystallization dynamics, as pMELTS calculations are all done at thermodynamic equilibrium (no time), and we do not model the separation of crystals and melt that becomes increasingly difficult at high crystal fraction [e.g., *Dufek and Bachmann*, 2010]. Pressure and volume changes implied by pure isobaric and isochoric crystallization are also often large enough to induce wall rock failure [e.g., *Fowler and Spera*, 2008], implying that other dynamics are also important. However, this procedure does provide bounds for the expected chemical evolution of LIP magma. Keeping track of the progressive concentration of volatiles in the melt phase, we test the solubility of volatiles at each temperature step (2 degrees). If saturation is reached, we calculate a mixture density of the melt phase via

$$\rho_{mix} = \left(\frac{n}{\rho_m} + \frac{1-n}{\rho_f}\right)^{-1}, \quad (1)$$

where n is the mass fraction of volatiles in the melt phase, ρ_m is the density of the melt calculated from pMELTS, and ρ_f is the density of the exsolved volatile phase (CO_2) as a supercritical fluid calculated via the MRK equation of state [*Kerrick and Jacobs*, 1981]. We vary the temperature and pressure (isochoric cases) according to the output of pMELTS to calculate H_2O + CO_2 solubility throughout the simulations, but use the initial melt composition throughout. This introduces errors in the solubility of order ~1%, negligible compared to other model approximations. Solid phases crystallizing from the melt are initially olivines and feldspars, with increasing amounts of plagioclase and pyroxene as crystallization progresses. We do not fractionate exsolved volatile phases, but note that the observation of diffuse CO_2 flux at ocean islands such as Hawaii [*Gerlach et al.*, 2002] implies that some phase separation does occur naturally.

[20] It is evident that significant melt buoyancy, calculated with respect to a fixed reference density of 2700 kg/m^3, is generated as fractionation proceeds (Figure 2a). At 800 MPa exsolution of CO_2 may not become a dominant control on density until roughly 35% crystallinity (isobaric upper bound), but the shallower 300 MPa experiment results in CO_2 exsolution even for zero crystallinity as the exsolution surface is at greater depth. This implies that magma reaching the Moho at shallow depths will be buoyant, with destabilization and eruption possible on a timescale proportional to the influx of primary melt. At greater depths the concentration of volatiles in the melt phase due to progressive fractionation will dictate the critical crystal fraction necessary to transition from ponding of magma to eruption. Isobaric experiments performed for volatile-free primitive magmas (blue and orange curves in Figure 2a) do not exhibit the same buoyancy production during crystallization and may stably pond even at shallow depths.

[21] LIP lava major element chemistry is another constraint on melt evolution, requiring some melt differentiation before eruption to generate basalt. We therefore use the liquid composition calculated from pMELTS to identify an additional possible threshold crystallinity for eruption. As Figure 2b illustrates, sufficiently evolved melts with basaltic MgO contents <10% [e.g., *Cox*, 1980; *Lange*, 2002] does not occur until ~25% crystallinity for both 300 MPa and 800 MPa.

[22] Given these bounds on the thermodynamic evolution of ponded primitive melts, we take 30% crystallinity to represent the transition from ponded to eruptible magmas based on buoyancy considerations, but experiment with a range of critical crystal fractions up to 80% to match the range of MgO contents observed in LIPs. We will show that the choice of critical crystal fraction is not a major control on the eruptibility of LIP magmas. However, lower choices of critical crystal fraction do imply additional fractionation during ascent or assimilation of surrounding crust to produce basalts. Sufficiently large influx of magma will cause net melting and assimilation to occur even at Moho depths. This latter

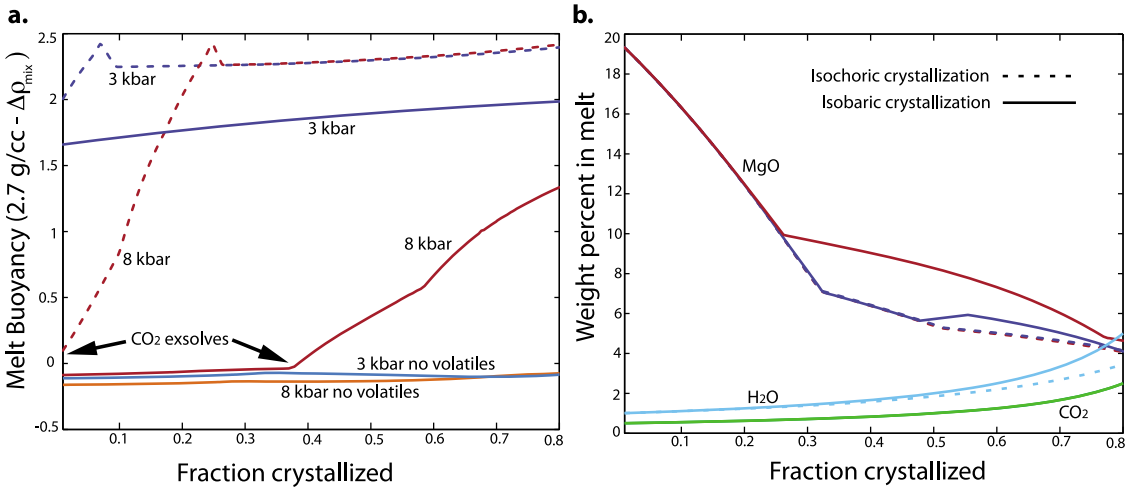

Figure 2. (a) Evolution of melt buoyancy during crystallization, with progressive volatile concentration and exsolution, at 300 MPa (blue curves, color in online version) and 800 MPa (red curves). Dashed lines are for isochoric crystallization, while solid lines are for isobaric crystallization. Buoyancy is calculated relative to 2700 kg/m^3, with exsolution of CO_2 at 800 MPa indicated by arrows. 300 MPa melts have exsolved CO_2 even at zero crystallinity. Mantle volatile contents of 0.1 wt% H_2O, 0.05 wt% CO_2 and ascent path described in the text are assumed. (b) Evolution of concentration for MgO in melt phase as a proxy for the chemical evolution of primitive magma. Concentration of CO_2 (green curve) and H_2O (blue curve) in the melt is similar at 3 and 800 MPa, but does vary slightly if crystallization is isochoric or isobaric.

effect may control the transition from dynamically stable to eruptible magma chambers at mid to upper crustal levels [*Karlstrom et al.*, 2010], facilitating intrusion of mafic melt into the lower crust. If assimilation does not contribute much to the buoyancy of these primitive melts, mantle melt influx will simply expand the chamber. When heat loss outpaces heat input to the chamber, fractional crystallization toward basaltic composition can occur.

[23] In summary, if the Moho acts as a mechanical trap for rising melts, primary magma reaching Moho depths is less dense than primary pyrolite but requires additional buoyancy production to continue rising through the lower crust. The timescale for this to occur depends on an interplay between crystal fractionation and volatile exsolution. At depths greater than the CO_2 saturation depth, the rate limiting process is volatile concentration through fractional crystallization of magma. At more shallow depths the rate limiting step is the accumulation of bubbly melt.

[24] Buoyancy production due to recharge of bubbly magma occurs on the filling timescale of the magma chamber, V_{ch}/Q, where V_{ch} is the chamber volume and Q is the melt influx. Chamber volumes are likely on the order of single eruptive volumes ($10^3 - 10^4$ km^3) [*Barry et al.*, 2010]. Melt flux (assuming rapid extraction of 10% partial melt from a plume head) scales with the ascent velocity V_{plume} of plume material across the rheological boundary layer of thickness Z at the base of the lithosphere as [e.g., *Sleep*, 2007] $Q \approx 0.1 V_{plume} A_{plume} \approx 0.1 \rho g \alpha \Delta T Z^2 \pi R_{plume}^2/\mu$. Influx ranges from $10^1 - 10^{-3}$ km^3/yr for $\Delta T = 100$ K, $\rho = 3000$ kg/m^3, $g = 10$ m/s^2, $\alpha = 10^{-5}$ K^{-1}, $Z = 10$ km, $\mu = 10^{17} - 10^{19}$ Pas and $R_{plume} = 100$ km (plume cross-sectional area is $A_{plume} = \pi R_{plume}^2$), thus the filling timescale is $\sim 10^2 - 10^6$ yr. We assume that filling times on the lower end of this range are reasonable for the present model.

[25] The timescale for fractional crystallization may also be simply estimated, by constructing the energy balance at the chamber walls that dictates the crystallization rate Q_{xtal}:

$$Q_{xtal} = \frac{q(\Delta T) S_{ch}}{\rho_{mix} L} - \frac{Q c_p \Delta T}{L}. \quad (2)$$

Here $q(\Delta T)$ is the heat flux at the walls, written explicitly as a function of temperature difference between chamber and country rocks, Q is the influx rate of magma into the chamber, and $Q_{xtal} = V_{xtal}/t_{xtal}$ is the rate of solidification in the chamber. S_{ch} the surface area of the chamber, taken to resemble an oblate spheroid, $c_p = 1.5$ KJ/kg K the specific heat capacity, ΔT a drop in temperature below the magma liquidus, and $L = 400$ KJ/kg the latent heat of fusion. Because the crystallized volume is a fraction of the total chamber volume ($V_{xtal} = \Phi V_{ch}$), we can rearrange equation (2) to find the time required to crystallize a fraction of the chamber volume at a given magma influx rate, plotted in Figure 3:

$$t_{xtal} = \Phi V_{ch} \left(\frac{q(\Delta T) S_{ch}}{\rho_{mix} L} - \frac{Q c_p \Delta T}{L} \right)^{-1}. \quad (3)$$

In equation (3) we experiment with $\Phi = 0.3 - 0.8$, the critical crystal fraction for eruptible magma as derived from our melt evolution calculations. This crystal fraction sets the melt mixture density ρ_{mix} and temperature drop ΔT between melt and country rocks. Larger ΔT corresponds to lower densities and shallower depths, while large mixture densities correspond to volatile poor, primitive melts at greater depth with smaller ΔT. The crystallization time t_{xtal} becomes large as input of enthalpy through magma influx approaches the dissipation of heat to the surroundings, which scales with the surface area of the chamber S_{ch} (Figure 3). This can be seen in

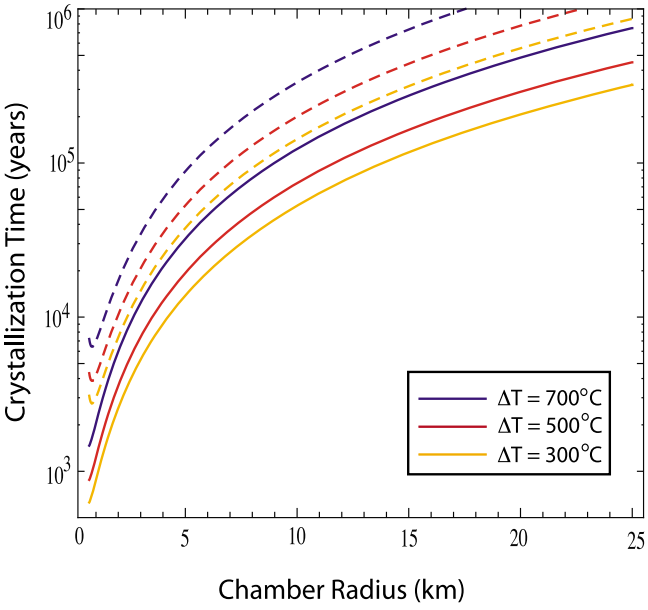

Figure 3. Buoyancy evolution timescale, taken to be the time until a critical fraction of the chamber has crystallized. Curves derive from equation (3) in the text, varying temperature difference between chamber and country rock. Magma influx is set to 10^{-2} km^3/yr. Larger magma influx values increase the incoming heat flux and thus increase the minimum chamber size required for crystallization. As discussed in the text, bounds for the critical crystal fraction are $\Phi = 0.8$ (dashed curves) in which fluid density $\rho_{mix} = 1500$ kg/m^3, and $\Phi = 0.3$ (solid curves) where $\rho_{mix} = 2700$ kg/m^3.

equation (3), where the crystallization time becomes singular as $q(\Delta T)S_{ch}/\rho_{mix}L \sim Qc_p\Delta T/L$.

[26] We estimate heat flux at the chamber walls using a steady state solution for a constant temperature oblate spheroid. Assuming large melt influx, this will underestimate heat transfer as it neglects the transient heating of an initially cool lower crust by the intrusion. It is an upper bound to the buoyancy evolution timescale. Steady state temperature around the chamber follows a simple expression in the oblate spheroidal coordinate system [*Moon and Spencer*, 1988]:

$$T(\mathbf{x}) = T(\xi) = T_0 + \Delta T \frac{\cot^{-1}(\xi)}{\cot^{-1}(\xi_0)}, \tag{4}$$

where $\xi \in [\xi_0, \infty]$ is a nondimensional distance from the chamber wall, and $\xi_0 = \sqrt{e^2 - 1}$ defines the boundary of an oblate spheroid with semimajor axis a, semiminor axis c and eccentricity $e = 1/a\sqrt{a^2 - c^2}$. T_0 is the background temperature, and ΔT is the temperature difference between the magma and country rocks. Heat flux is then, with $k = 3 - 4$ W/m^2 the thermal conductivity [*Whittington et al.*, 2009],

$$q(\xi) = k\nabla T(\xi) = \frac{k\Delta T}{\cot^{-1}(\xi_0)(1+\xi^2)}\left[\frac{1+\xi^2}{(a^2-c^2)(\xi^2+\eta^2)}\right]^{1/2}, \tag{5}$$

where $\eta \in [-1, 1]$ is the polar angle in the oblate spheroidal coordinate system. This heat flux closely approximates a heated sphere at large distances, but reflects geometrical differences in the near field and is larger at the poles than at the equator (Figure 4a). Using surface area

$$S_{ch} = 2\pi a^2 + \pi\frac{c^2}{e}\ln\left(\frac{1+e}{1-e}\right) \tag{6}$$

and volume $V_{ch} = 4/3\pi a^2 c$ we can then use equation (3) to estimate the time required to obtain an eruptible, basaltic composition magma. After this time, magma can rise through the lower crust, driven by a combination of buoyancy and overpressure. However, as Figure 3 illustrates, the ultimate choice of critical crystal fraction for which buoyant melts is fairly unimportant. Comparing calculations for $\Phi = 0.3$, $\rho_{mix} = 2700$ kg/m^3 (solid curves) with those for $\Phi = 0.8$, $\rho_{mix} = 1500$ kg/m^3 (dotted curves), we find that the predicted timescales are roughly linear in Φ. The timescale for buoyancy

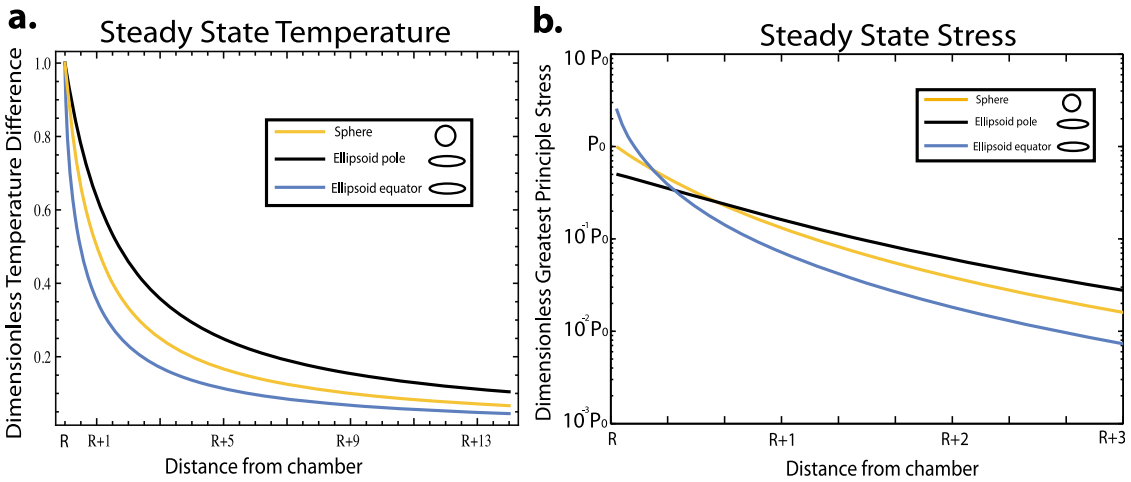

Figure 4. Comparison between a sphere and oblate spheroid with aspect ratio = 0.1. (a) Steady state temperatures in an infinite medium. For the spheroid polar heat transfer is enhanced relative to a sphere, while equatorial heat transfer is diminished. (b) Steady state greatest principle deviatoric stress in an infinite medium. Overpressure is set to P_0 at the chamber wall.

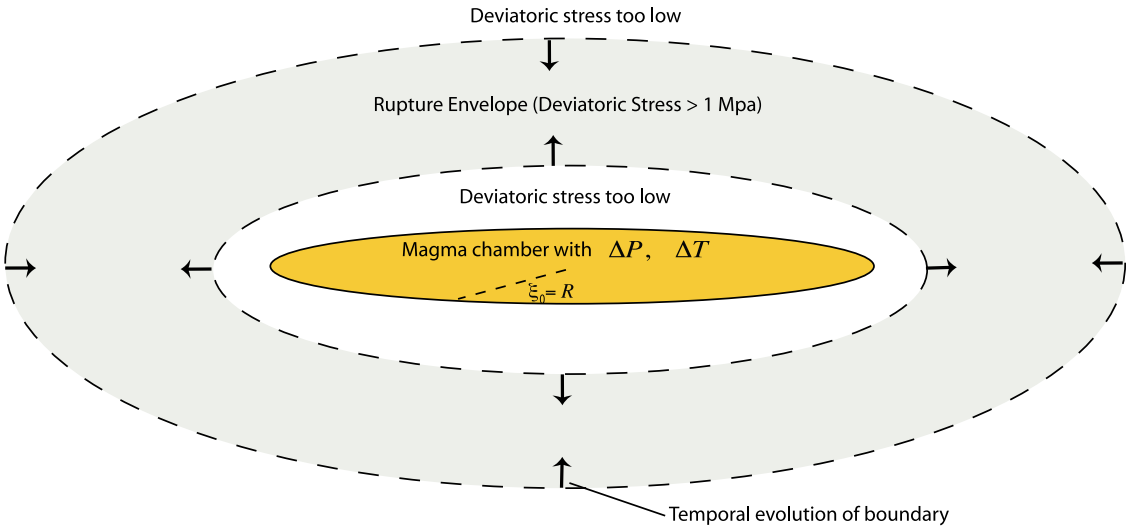

Figure 5. Thermomechanical model for time dependent stresses around a hot, pressurized magma chamber, defined by the curve $\xi_0 = R$. Initial deviatoric stresses from overpressured magma create a rupture envelope that surrounds the chamber, in which the critical stress required for dike formation is exceeded. Viscous creep induced by gradual heating of country rocks relaxes away deviatoric stresses and eventually inhibits dike formation.

evolution will be less than 1 Ma for all reasonable parameter choices.

5. Magma Chamber Dynamics

[27] We now consider the eruptive evolution of an LIP magma chamber. Assuming that isotropic overpressure is the dominant stress boundary condition, we follow the conceptual magma chamber model of *Jellinek and DePaolo* [2003], who proposed that prolonged heating of country rocks produces a shell of viscoelastic material that may undergo viscous creep on the timescale of chamber pressurization, relaxing away deviatoric stresses in the country rocks. These stresses are responsible for fracture and dike generation, so viscoelastic relaxation is a mechanism by which chambers may grow and remain stable at temperatures above the solidus without eruption for extended timescales [*Jellinek and DePaolo*, 2003; *Karlstrom et al.*, 2010].

[28] We assume a threshold propagation criterion for dike propagation in which dikes may form if deviatoric stresses in the country rocks exceed a critical value of 1 MPa [*Rubin*, 1995]. This is a crude approximation to dike propagation mechanics, but it does allow us to explore the relevant timescales for stress relaxation and dike shutoff implicit in our hypothesis. Initial deviatoric stresses in the country rocks larger than 1 MPa are spatially concentrated around the chamber in a rupture envelope (Figure 5), bounded by the geometric falloff and relaxation of deviatoric stresses. The region of viscous creep expands in time as heat diffuses from the chamber, so effective viscoelastic relaxation is time-dependent and the rupture envelope progressively shrinks. The time at which deviatoric stresses everywhere relax below 1 MPa is taken to be the maximum timescale over which dike propagation can occur.

[29] Magma chambers are often idealized as pressurized cavities in elastic or viscoelastic media [*Gudmundsson*, 2006]. Stresses generated by a pressurized oblate spheroidal magma chamber are modeled with the equations of linear elasticity with no body force [e.g., *Fung*, 1965], subject to the normal stress boundary conditions at the boundary of the chamber R. We use a numerical implementation of the exact solution to this problem [*Eshelby*, 1957; *Healy*, 2009], illustrated in Figure 4b.

[30] Stresses are then related to the thermal evolution of rocks around the magma chamber, through a Maxwell viscoelastic constitutive equation for the country rocks. Maxwell viscoelastic stress solutions are available for pressurized chambers with simple geometry [e.g., *Dragoni and Magnanensi*, 1989; *Karlstrom et al.*, 2010], and exhibit exponential relaxation of deviatoric stresses on a characteristic (Maxwell) timescale $\tau = C\mu/Y$, where μ is the viscosity of the wall rocks, Y is the Young's Modulus, and C is a geometrical factor (of order unity) related to the size and shape of the viscoelastic shell. We assume that time dependent deviatoric stresses $\sigma_{dev}(x, t)$ for our problem take the form

$$\sigma_{dev}(x,t) \approx \sigma_{dev}(x) \exp\left(-\frac{t}{\tau}\right), \tag{7}$$

and that we can use the static Eshelby solution to calculate $\sigma_{dev}(x)$.

[31] Viscosity follows an Arrhenius law

$$\mu = A^{-1/n} \exp\left(\frac{E}{nRT(\mathbf{x},t)}\right), \tag{8}$$

in which A depends on the particular stress-strain relation used, R is the ideal gas constant, E is an activation energy, and n is the power law exponent. E and n depend upon confining pressure and rock type, while A in our parameterization depends on grain size (taken to be constant at 100 μm). We refer to several sets of laboratory dislocation creep measurements on mantle lithosphere and lower crustal rocks to

Table 1. Rheological Parameters[a]

Mineralogy	log A ($MPa^{-n}\mu m^m\ s^{-1}$)	G (kJ/mol)	n	m
Dry anorthite[b]	$10^{12.1}$	467	1	3
Wet anorthite[b]	$10^{1.7}$	170	1	3
Dry clinopyroxene[c]	$10^{15.1}$	560	1	3
Wet clinopyroxene[d]	$10^{6.1}$	340	1	3
Dry olivine[e]	$10^{6.1}$	510	3	0
Wet olivine[e]	$10^{2.9}$	470	3	0

[a]For those cases where m > 0, we take a nominal grain size of 100 μm.
[b]*Rybacki and Dresen* [2000].
[c]*Bystricky and Mackwell* [2001].
[d]*Hier-Majumder et al*. [2005].
[e]*Karato and Jung* [2003].

bracket the rheological behavior at Moho depths (Table 1), including data on pyroxenite, olivine and anorthite. Rheology is of critical importance to our results, although there is significant uncertainty in the appropriate Arrhenius parameters n, E, and A for the lower crust [*Bürgmann and Dresen*, 2008].

[32] We cannot assume steady state heat transfer, as we did to estimate a crystallization time of the magma chamber. However, the available asymptotic analytic solutions [*Norminton and Blackwell*, 1964; *Blackwell*, 1972] are not sufficient. We assume an idealized temperature evolution, the sudden heating of a sphere with radius equal to the semimajor axis of our ellipse:

$$T(\mathbf{x},t) = T(r,t) = T_0 + \Delta T \frac{R_c}{r}\,\mathrm{erfc}\left(\frac{r-R_c}{2\sqrt{\kappa t}}\right), \qquad (9)$$

where T_0 is the initial temperature of the wall rocks, ΔT is the temperature change imposed by the magma chamber, R_c is the radius and r is distance from the of the sphere, $\kappa = 0.5 \times 10^{-6} m^2/s$ [*Whittington et al*., 2009] is the thermal diffusivity and t is time. This solution overestimates thermal diffusion near the midplane of a spheroidal magma chamber (see the steady state temperatures in Figure 4a). Given our neglect of other important transient heat transfer processes such as crystallization and convection within the chamber [e.g., *Marsh*, 1989], however, this model is sufficient.

[33] We combine equations (7)–(9) to estimate the temporal evolution of the temperature and stresses surrounding the magma chamber. Effective deviatoric stresses are doubly exponential functions of temperature

$$\sigma_{dev}(x,t) \approx \sigma_{dev}(x)\exp\left[-t\ YA^{1/n}\exp\left(\frac{-E}{nRT(\mathbf{x},t)}\right)\right]. \qquad (10)$$

[34] In general viscosity depends on stress as well as temperature [e.g., *Jull and Kelemen*, 2001], but the doubly exponential temperature dependence should dominate the relaxation behavior, and this fact leads to rather robust limits on the timescale over which deviatoric stresses around a heated and pressurized magma body are effectively dissipated.

6. External Triggers

[35] Finally, we consider the possibility that large igneous province magma chambers might be destabilized by stresses imposed externally. There are two sources for these stresses. First, background tectonics or flexure of the lithosphere due to plume emplacement may generate stress concentration around a magma chamber, and may facilitate transport of magma to higher crustal levels or the surface. We neglect tectonic forcing here, but note that plume-related flexural stresses should induce sill emplacement and horizontal transport of magma rather than surface eruption, due to the subhorizontal orientations of principle stresses in the bottom half of the plate [*Galgana et al*., 2011]. This could be a source of large-scale sill emplacement if dynamic topography increases throughout the eruptive process.

[36] An additional source of external stresses is the Earth's free surface: as is well known, a pressurized cavity beneath a free surface incurs shear stresses that concentrate along the margins of the chamber. This effect is often invoked as the source of ring fractures during caldera collapse [*Gudmundsson*, 1998], and becomes pronounced when the ratio of chamber size to chamber depth approaches unity [*Grosfils*, 2007]. Free surface stresses may also be important for the dynamic organization of deeper crustal melt transport [e.g., *Karlstrom et al*., 2009].

[37] It is possible that LIP magma reservoirs, despite their depth, may grow laterally large enough for free surface stresses to become important. In this case, free surface stresses place a fundamental limit on the size (and eruptible volume) of these chambers. We assume here for simplicity that dike formation occurs when the lateral chamber dimension is equal to the depth. These shear stresses will not be relaxed away through viscous creep unless the entire crust behaves as a Newtonian fluid on the timescale of magma transport, hence there is a basic mechanistic limit on the size of a continuous overpressured body at depth.

7. Results

[38] Shutoff timescales implied by equation (10) are evaluated for a range of magma chamber sizes and rheological parameters using Newton-Raphson iteration. The maximum stress occurs at the midplane of the oblate spheroid, where curvature is highest. We calculate the maximum deviatoric stress as a function of distance from the chamber, and evolve time forward to find the longest time for which stresses around the chamber exceed 1 MPa (Figure 5). Magma chamber overpressure may be estimated in a variety of ways, but is in general a major uncertainty in the modeling of magma dynamics. We choose an overpressure of 100 MPa in all models. Although transient stresses larger than this value might be possible, 100 MPa exceeds most estimates of maximum magma chamber failure strength [e.g., *Jellinek and DePaolo*, 2003; *Traversa et al*., 2010] and will result in the redistribution of melt through diking rather than prolonged storage in a central reservoir. The influx rates implied by this overpressure are a function of chamber volume, but generally fall in the range of $10^0 - 10^{-3}$ km^3/yr.

[39] To close the thermal part of the model, we have assumed a Moho level emplacement in continental and oceanic crust. These end-member scenarios provide a guide for the expected background temperatures, pressures, and country rock rheologies. Although there is considerable controversy over the dominant structure and deformation

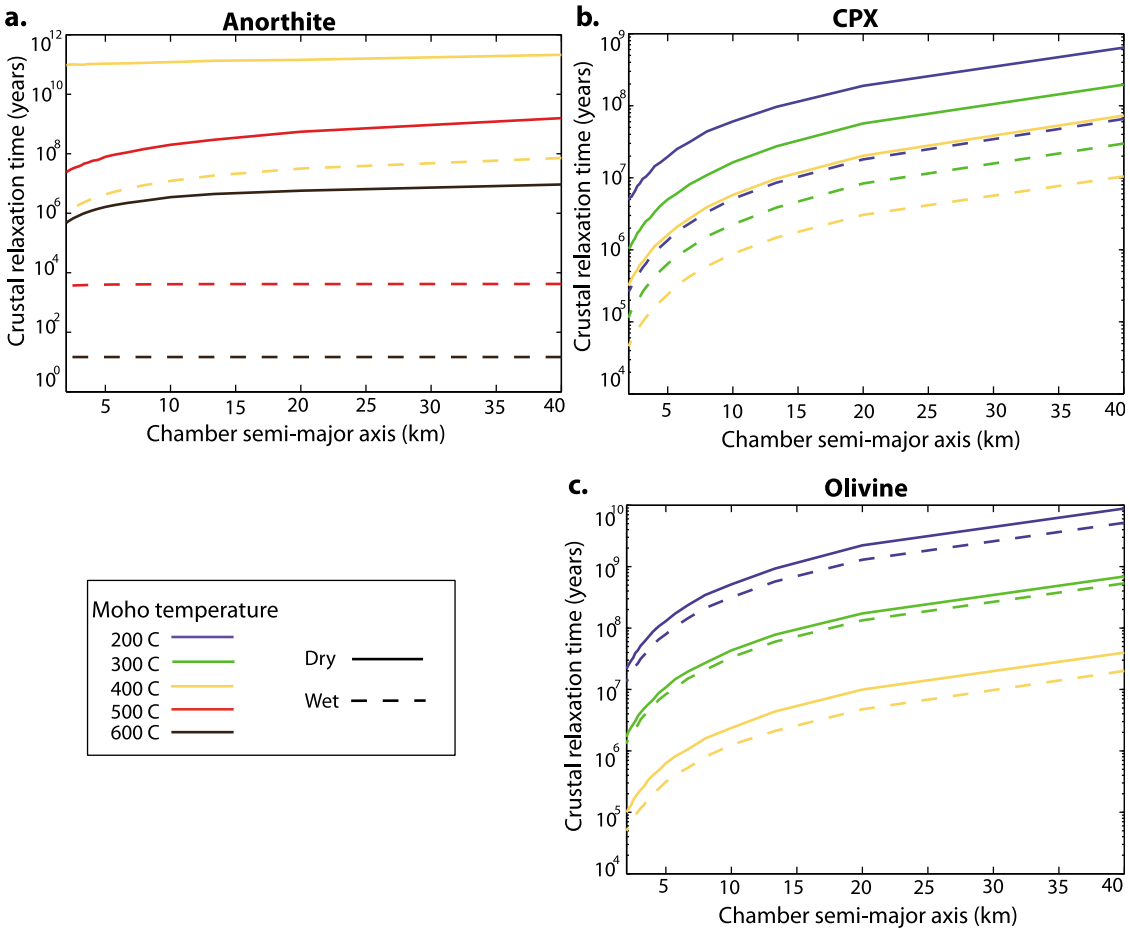

Figure 6. Time until deviatoric stresses relax below 1 MPa everywhere around the chamber, as evaluated from equation (10). Curves are for different temperature contrast between intruded magma and crust (as proxy for varying Moho temperatures in continental and oceanic settings), calculated for power law rheological parameters of (a) anorthite, (b) clinopyroxene, and (c) olivine. Dashed curves correspond to equivalent but hydrated mineralogy (Table 1).

mechanisms of the lower (particularly continental) crust [e.g., *Bürgmann and Dresen*, 2008], different hypotheses may be simplified into two scenarios: hot and dry or cool and wet lower crustal rheologies. We perform calculations for both cases, assuming experimentally determined power law parameters for anorthite, clinopyroxene and olivine to explore the likely parameter space (Table 1).

[40] The maximum time over which stresses anywhere outside the chamber exceed 1 MPa is found by testing a range of Moho temperatures and chamber sizes (fixing chamber aspect ratio = 0.1). As a consequence of the doubly exponential dependence of deviatoric stresses on temperature, initial Moho temperature exerts the strongest control on this timescale. Continental crust is represented by an initial temperature difference of 600–800°C between Moho and intruding magma depending on choices of intrusion depth and surface heat flow in the conductive geothermal gradient (Figure 6a). Using a typical conductive geothermal gradient, these temperatures map onto crustal thicknesses of 30–50 km. High velocity layers commonly exist at ~40 km depths beneath continental provinces (Moho temperatures of ~530°C) [*Ridley and Richards*, 2010]. Oceanic crust is thinner (average thickness 7 km), with higher heat flow and an error function geothermal gradient, resulting in larger temperature differences of 700–900°C between melt and country rocks (Figure 6b) corresponding to Moho depths of 10–30 km. High velocity layers are commonly observed at ~20 km depths under oceanic LIPs [*Ridley and Richards*, 2010].

[41] As Figure 6 emphasizes, country rock rheology (as expressed through the Arhennius parameters n, E, and A in Table 1) has first order effects on relaxation times. While the list of plausible crustal rheological parameters in either case is long [*Bürgmann and Dresen*, 2008], the range of relaxation times here provides a rough guide to effects of composition. We also model the effect of water in both cases (dotted curves in Figure 6), illustrating that hydrated mineral assemblages will relax away deviatoric stresses with greater ease than their dry counterparts. Overall, we find that hotter emplacement temperatures and hydrated mineralogies are most consistent with relaxation times of order 10^6 years for both continental (some combination of anorthite and anorthite and clinopyr-

oxene) and oceanic (clinopyroxene and olivine) settings. Chamber size exerts some control on the relaxation timescale, with smaller chambers representing smaller stress perturbations than larger chambers, but overall this is a secondary effect compared to environmental conditions.

8. Controls on Critical Chamber Size

[42] We now assess which of the three mechanisms for chamber destabilization presented here (elastic pressurization, buoyancy evolution, free surface effects) may be important for LIPs. Chemical evolution must occur before main stage eruptions can begin, as LIPs are often predominately basalt. By comparing Figures 3 and 6, it is evident that under many circumstances chemical evolution occurs rapidly, followed by chamber failure that is eventually shut off due to relaxation of deviatoric stresses on a timescale similar to the main stage of many LIPs. Crustal relaxation times vary considerably depending on lower crustal rheology (Figure 6), however assuming hot, dry continental lower crust and cool, wet oceanic crust, it is quite reasonable to infer a relaxation (or equivalently an eruptive) timescale of $\sim 10^6$ years in both cases.

[43] Nonetheless, there are also clearly cases for which isotropic stresses may be relaxed much more quickly. It is possible in some circumstances that buoyancy evolution is outpaced by viscous relaxation of stresses, and other mechanisms for destabilizing LIP magma chambers must operate. In a viscous regime in which continued influx does not induce eruptions through diking, LIP chambers will spread out along the Moho as gravity currents. Recharge related deviatoric stresses decay quickly in this regime, and the chamber will continue to stably expand until free surface shear stresses begin to accumulate around the chamber. For an axisymmetric viscous gravity current, the semi major axis a will scale with time as $a \approx Kt^n$, with K, n positive constants that depend on the boundary conditions, material properties and input flux [*Lister and Kerr*, 1989]. $n = 1/2$ for steady axisymmetric flow along a rigid boundary fed by constant flux Q, while $K = (g'Q^3/\mu)^{1/8}$ with μ the viscosity of the surrounding liquid (the warmed wall rocks), and g' gravity scaled by the density difference between the fluid and the surroundings.

[44] Assuming a density difference of 300 kg/m^3, ambient viscosities of $\mu = 10^{16} - 10^{20}$ Pas, and a range of melt influx $Q = 10^0 - 10^{-3}$ km^3/yr, this scaling suggests that in a viscous regime, magma spreading at the Moho will attain a length scale comparable to its depth in $\sim 0.1 - 1$ million years. At this point we assume that elastic stresses due to free surface effects accumulate, initiating melt redistribution and eruptions. Progressive warming will lead to increased viscous response of the country rock, thus this mechanism provides a limit to the stable size of magma chambers, redistributing stored melt through diking or surface eruptions. However, there is no simple way to shut off eruptions via this mechanism, so surface eruptions would continue unimpeded for the duration of mantle melting. Based on the evidence for crustal modulation of mantle melting represented by distinct main phase eruptions, we rule out a purely viscous response to lower crustal melt flux. But such considerations do suggest the possibility of entirely intrusive LIPs that never erupt large volumes of lava.

9. Discussion

[45] Provided melt extraction from the mantle is rapid, our analysis suggests that modulation of magma transport by the crust controls the progression of large igneous province eruptions. The other end-member hypothesis, that surface emplacement of lavas tracks decompression melting evolution, is hard to reconcile with the observed timing and volume of main phase eruptions [e.g., *Hooper et al*., 2007] and the presence of cumulate layers at Moho depths beneath most flood basalt provinces [*Ridley and Richards*, 2010]. However, we recognize that the dynamics of plume/lithosphere interaction are significantly more complex than we assume here. Possible multiple maxima in plume head melting due to thermochemical effects [*Leitch and Davies*, 2001; *Lin and van Keken*, 2005], and deflection of plume material by Moho level topography due to cratonic keels [*Sleep et al*., 2002] or passive continental margins [*Sleep*, 2007] may modulate the evolution of pressure release melting during plume emplacement. Low matrix permeabilities will slow melt extraction and induce buoyant convective instabilities in the melting region [*Hernlund et al*., 2008] providing a possible melting feedback in the dynamics of plume-lithosphere interactions and well as possible episodic supply [*Schmeling*, 2006].

[46] These processes are beyond the scope of this work, but may be important in a more complete integration of LIP phenomenology. We assume that decompression melting follows a simple single maximum trend, and that the scaling of section 4 for supply of ultramafic melt from the plume source to the lower crust holds over the timescale of many eruptions. This then provides the background supply for cyclic magma chamber filling and draining and controls the episodicity of surface eruptions.

[47] Our analysis suggests two fundamental destabilization mechanisms for LIP magma reservoirs, given sufficient buoyancy to make the magmas eruptible. After the emplacement of magma at the Moho, the elastic response of country rocks initially allows fracture and dike propagation that accommodates the overpressure of rising melts. The length of this period of elastic behavior depends on country rock rheology, background stresses and the initial geothermal gradient, which varies between continental and oceanic settings. We propose that the main phase of LIP emplacement occurs during this time window, constraining the rheology of the lower crust to mineral assemblages that, upon heating, may relax away deviatoric stresses in ~1 Ma. For continental crust we find that either cool and wet or hot and dry combinations of anorthite and clinopyroxene will satisfy this constraint (Figures 6a and 6b). For thinner oceanic crust hydrated mafic mineralogy is more suitable (Figures 6b and 6c). The record of large-scaleigneous events may in this way reflect the rheological structure and evolution of the crust.

[48] After prolonged warming has occurred viscous relaxation of stresses dominates and magma chambers will grow stably without erupting. Limits to this growth may come from more rapid differentiation of magma in time, or from external sources of stress such as those exerted on the chamber by the

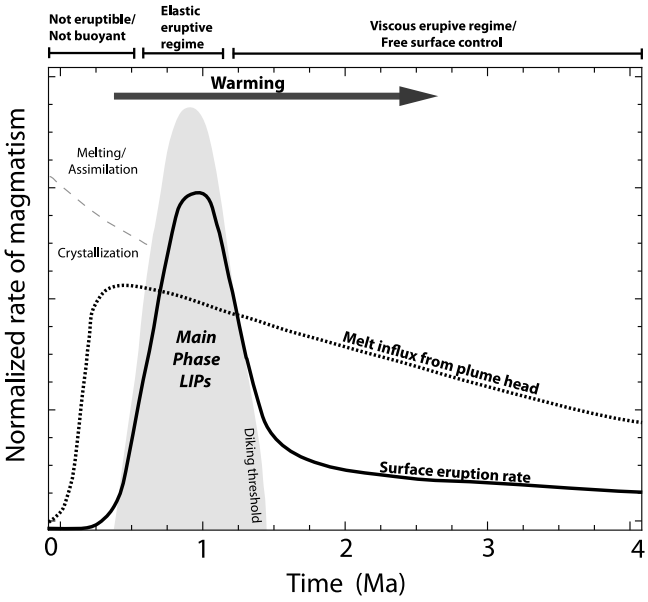

Figure 7. Qualitative regimes of LIP magmatism, with curves illustrating inferred eruption rate of the Columbia River Flood Basalt province [*Hooper et al*., 2007] and simplified evolution for generic LIP primary melt generation [*Leitch and Davies*, 2001]. Initial intrusive magmatism is associated with chemical evolution of Moho level primary melts along with possible assimilation of crustal material, while the transition between largely extrusive and intrusive magmatism after ~1 Ma of main phase eruptions reflects the onset of viscous creep in the lower crust. Free surface control provides a destabilizing trigger for eruptions in the viscous regime. Shaded gray region denotes a regime in which sufficiently cool crust promotes dike propagation and surface eruption of stored magma.

free surface. This latter mechanism places a constraint on the size of a magma reservoir set by the length scale over which stable growth can occur (section 5): lateral size will scale with the depth of the reservoir, and implies that magma chambers residing below crust of different thickness, such as oceanic versus continental settings, have different maximum sizes. If individual LIP eruption volumes scale with magma chamber size, this predicts larger flows in continental provinces. Large background stresses may also be important for LIPs: preserved surface feeder dikes are largely linear in nature perhaps implying local extension in some provinces [*Ray et al*., 2007], while deep radial dike swarms perhaps associated with plume head emplacement can be thousands of kilometers long [*Ernst and Buchan*, 1997] and might broadly distribute primary melt.

10. Model for LIP Crustal Magma Transport

[49] In our model the progression of LIP emplacement begins with intrusive early magmatism, transitioning to a short largely extrusive main stage, then back to an intrusion-dominated regime that lasts for the duration of melt supply. Figure 7 illustrates this model qualitatively, through comparison of simulated plume head melting rates (modified from *Leitch and Davies* [2001]) and the inferred extrusion rate from the Columbia River Flood Basalt Province [*Hooper et al*., 2007]. These curves are qualitative, meant to illustrate the transitions in style of magmatism during LIPs in the framework of starting plume-lithosphere interactions.

[50] Upon emplacement, chemical evolution from ultramafic to basaltic melt occurs. Mantle plume melts formed at sublithospheric depths will be more dense than typical mafic lower crustal rocks, and should therefore pond at the Moho or within the lower crust, undergoing extensive fractionation of mainly olivine and pyroxene before evolving large volumes of basaltic liquids able to rise to the surface. The duration of this fractionation phase depends on the melt flux and heat transfer out of the lower crust. There may be a period of melting and assimilation during high flux phases of melt emplacement before fractional crystallization can occur to further evolve the bulk of the melt (Figure 7, top left).

[51] Next, brittle fracture of the lower crust due to stresses generated by the lower crustal basaltic magma reservoir induces dike emplacement and the main phase of LIP surface eruptions. This elastic phase depends strongly on the rheology of the lower crust; for sufficiently warm and/or weak country rocks it may be absent (Figure 7, top), suggesting the possibility of noneruptive LIPs. This phase is relatively insensitive to the flux of magma, however, assuming that large reservoirs of basaltic melt exist.

[52] Finally, viscous response of the lower crust stabilizes magma chambers, and they spread gravitationally until buoyancy or external triggers cause local disruption and elastic failure. We hypothesize that the accumulation of free surface stresses for laterally extensive LIP chambers limits their size. The viscous regime lasts the lifetime of melt supply, likely accompanied by dynamic surface topography as intrusions accumulate in the lower crust.

[53] Throughout the lifetime of continued primitive melt flux, progressively more buoyant melt will move upward from the Moho, directed by the continued background stresses of plume impingement on the lithosphere. Emplaced through elastic failure of country rocks on short timescales, they will form a dense network of intrusions that, once frozen, put the lower crust into compression that is only relaxed through plate-scale spreading or viscous creep. This induces horizontal magma transport and sill emplacement that likely moves upward through time [*Parsons et al*., 1992] (Figure 1). Examples of such intrusion networks are observed, e.g., in the Ferrar LIP dolerite sills of Antarctica [*Elliot and Fleming*, 2008].

[54] Individual LIP eruptions (which may reach volumes of $\leq 10^4$ km^3) are discrete in space and time, although the total erupted volumes are not well constrained in many cases [e.g., *Mangan et al*., 1986; *Bryan et al*., 2010]. The model here is consistent with a scenario in which individual eruptions tap individual magma chambers during the main phase. The timescale between eruptions would reflect the timescale for buildup of significant deviatoric stress in the lower crust, set by the recharge timescale and the production of buoyancy due to volatile exsolution. Deep exsolution of CO_2 can destabilize chambers at relatively low crystal fractions (<35%) even at 30–40 km depths as magma differentiation proceeds (Figure 2).

[55] Massive ultramafic intrusive complexes at Moho depths suggest that the largest fraction of magmas from the mantle may never rise above the lower most crust. Models for

LIPs must directly address the processes associated with these deep magma bodies, especially the possible modes by which more evolved magmas may escape to generate surface eruptions and, perhaps, shallower magma bodies. We have shown that simple scaling considerations for viscoelastic deviatoric stress relaxation around a sill-like magma chamber due to progressive heating can explain a main stage eruptive timescale of ~1 Ma, with continued magma emplacement over the ~10 Ma mantle melting timescale.

[56] Because the rheology of lower crustal rocks plays a fundamental role in setting the viscoelastic relaxation timescale (Figure 6), reconstructions of surface lava output through the cessation of main phase eruptions [e.g., *Barry et al*., 2010] might provide a means of constraining lower crustal rheology. It is possible even that the spatial heterogeneity in lower crustal rocks may account for much of the variability observed among flood basalt provinces, between oceanic and continental settings and between continental LIPs emplaced through accreted terrains or stable cratonic settings [*Wolff et al*., 2008].

[57] Our model offers three distinct hypotheses for the evolution and distribution of LIP magmas: (1) Main phase eruptions are shut off when viscous creep overwhelms elastic failure as the primary mechanism of relieving stresses in the lower crust (2) The lateral extent of individual high melt fraction, mafic magma chambers is limited by their depth of emplacement (3) The magmatic plumbing of LIPs moves upward in time, forming a network of individual sills that populate the lower crust. This causes continued dynamic topography over the lifetime of melt supply, as the rheology of the lower crust responds to magmatic input of heat and stress.

[58] **Acknowledgments.** The authors thank Norman H. Sleep and Shan de Silva for insightful reviews and NASA grant NNX09AN18G.

References

Allegre, C., J. Birck, F. Capmas, and V. Courtillot (1999), Age of the Deccan traps using ^{187}Re-^{187}Os systematics, *Earth Planet. Sci. Lett.*, *170*, 197–204.

Asimow, P., and M. Ghiorso (1998), Algorithmic modifications extending melts to calculate subsolidus phase relations, *Am. Mineral.*, *83*, 1127–1132.

Barry, T., S. Self, S. Kelley, S. Reidel, and P. Hooper (2010), New ^{40}Ar/^{39}Ar dating of the Grande Ronde lavas, Columbia River basalts, USA: Implications for duration of flood basalt eruption episodes, *Lithos*, *118*, 213–222.

Blackwell, J. (1972), Transient heat flow from a thin circular disk—Small-time solution, *J. Aust. Math. Soc.*, *14*(4), 433–442.

Brooks, C. (1973), Rifting and doming in southern East Greenland, *Nature*, *244*, 23–25.

Brooks, C. (1982), The E. Greenland continental-margin: A transition between oceanic and continental magmatism, *J. Geol. Soc.*, *139*, 265–175.

Bryan, S. E., I. U. Peate, D. W. Peat, S. Self, D. A. Jerram, M. R. Mawby, J. S. Marsh, and J. A. Miller (2010), The largest volcanic eruptions on Earth, *Earth Sci. Rev.*, *102*, 207–229.

Bürgmann, R., and G. Dresen (2008), Rheology of the lower crust and upper mantle: Evidence from rock mechanics, geodesy, and field observations, *Annu. Rev. Earth Planet. Sci.*, *36*, 531–567.

Burov, E., L. Guillou-Frottier, E. d'Acremont, L. L. Pourhiet, and S. Cloetingh (2007), Plume head-lithosphere interactions near intra-continental plate boundaries, *Tectonophysics*, *434*(1–4), 15–38.

Bystricky, M., and S. Mackwell (2001), Creep of dry clinopyroxene aggregates, *J. Geophys. Res.*, *106*, 13,443–13,454.

Campbell, I., and R. Griffiths (1990), Implications of mantle plume structure for the evolution of flood basalts, *Earth Planet. Sci. Lett.*, *99*, 79–93.

Coffin, M., and O. Eldholm (1994), Large igneous provinces: Crustal structure, dimensions, and external consequences, *Rev. Geophys.*, *32*(1), 1–36.

Contreras-Reyes, E., I. Grevemeyer, and A. Watts (2010), Crustal intrusion beneath the Louisville hotspot track, *Earth Planet. Sci. Lett.*, *289*, 323–333.

Courtillot, V., and P. Renne (2003), On the ages of flood basalt events, *C. R. Geosci.*, *335*, 113–140.

Cox, K. (1980), A model for flood basalt vulcanism, *J. Petrol.*, *21*(4), 629–650.

Dasgupta, R., and M. M. Hirschmann (2006), Melting in the Earth's deep upper mantle caused by carbon dioxide, *Nature*, *440*, 659–662.

de Silva, S. L., and W. D. Gosnold (2007), Episodic construction of batholiths: Insights from the spatiotemporal development of an ignimbrite flare-up, *J. Volcanol. Geotherm. Res.*, *167*, 320–335.

Dragoni, M., and C. Magnanensi (1989), Displacement and stress produced by a pressurized, spherical magma chamber, surrounded by a viscoelastic shell, *Phys. Earth Planet. Inter.*, *56*, 316–328.

Dufek, J., and O. Bachmann (2010), Quantum magmatism: Magmatic compositional gaps generated by melt-crystal dynamics, *Geology*, *38*(8), 687–690.

Elliot, D., and T. Fleming (2008), Physical volcanology and geological relationships of the Jurassic Ferrar large igneous province, Antarctica, *J. Volcanol. Geotherm. Res.*, *172*, 20–37.

Ernst, R. L., and K. L. Buchan (1997), Giant radiating dyke swarms: Their use in identifying pre-Mesozoic large igneous provinces and mantle plumes, in *Large Igneous Provinces: Continental, Oceanic, and Planetary Flood Volcanism*, *Geophys. Monogr. Ser.*, vol. 100, pp. 297–332, AGU, Washington, D. C.

Eshelby, J. (1957), The determination of the elastic field of an ellipsoidal inclusion, and related problems, *Proc. R. Soc. A*, *241*, 376–396.

Farnetani, C., and H. Samuel (2005), Beyond the thermal plume paradigm, *Geophys. Res. Lett.*, *32*, L07311, doi:10.1029/2005GL022360.

Farnetani, C., M. Richards, and M. Ghiorso (1996), Petrological models of magma evolution and deep crustal structure beneath hotspots and flood basalt provinces, *Earth Planet. Sci. Lett.*, *143*, 81–94.

Farnetani, C. G., and M. A. Richards (1994), Numerical investigations of the mantle plume initiation model for flood basalt events, *J. Geophys. Res.*, *99*, 13,813–13,833.

Feighner, M., and M. Richards (1994), Lithospheric structure and compensation mechanisms of the Galapagos archipelago, *J. Geophys. Res.*, *99*, 6711–6729.

Fowler, S. J., and F. J. Spera (2008), Phase equilibria trigger for explosive volcanic eruptions, *Geophys. Res. Lett.*, *35*, L08309, doi:10.1029/2008GL033665.

Fung, Y. C. (1965), *Foundations of Solid Mechanics*, Prentice-Hall, Englewood Cliffs, N. J.

Furlong, K. P., and D. M. Fountain (1986), Continental crustal underplating: Thermal considerations and seismic-petrologic consequences, *J. Geophys. Res.*, *91*, 8285–8294.

Galgana, G. A., P. J. McGovern, and E. B. Grosfils (2011), Evolution of large venusian volcanoes: Insights from coupled models of lithospheric flexure and magma reservoir pressurization, *J. Geophys. Res.*, *116*, E03009, doi:10.1029/2010JE003654.

Geist, D., T. Naumann, and J. Standish (2005), Wolf volcano, Galápagos archipelago: Melting and magmatic evolution at the margins of a mantle plume, *J. Petrol.*, *46*(11), 2197–2224.

Gerlach, T. M., K. A. McGee, T. Elias, A. J. Sutton, and M. P. Doukas (2002), Carbon dioxide emission rate of Kilauea volcano: Implications for primary magma and the summit reservoir, *J. Geophys. Res.*, *107*(B9), 2189, doi:10.1029/2001JB000407.

Ghiorso, M., and R. Sack (1995), Chemical mass transfer in magmatic processes IV: A revised and internally consistent thermodynamic model for the interpolation and extrapolation of liquid-solid equilibria in magmatic systems at elevated temperatures and pressures, *Contrib. Mineral. Petrol.*, *119*, 197–212.

Ghiorso, M., M. Hirschmann, and P. Reiners (2002), The pMELTS: A revision of melts for improved calculation of phase relations and major element partitioning related to partial melting of the mantle to 3 GPa, *Geochem. Geophys. Geosyst.*, *3*(5), 1030, doi:10.1029/2001GC000217.

Grosfils, E. (2007), Magma reservoir failure on the terrestrial planets: Assessing the importance of gravitational loading in simple elastic models, *J. Volcanol. Geotherm. Res.*, *166*, 47–75.

Gudmundsson, A. (1998), Formation and development of normal-fault calderas and the initiation of large explosive eruptions, *Bull. Volcanol.*, *60*, 160–170.

Gudmundsson, A. (2006), How local stresses control magma-chamber ruptures, dyke injections, and eruptions in composite volcanoes, *Earth Sci. Rev.*, *79*, 1–31.

Hales, T., D. Abt, E. Humphreys, and J. Roering (2005), A lithospheric instability origin for columbia river flood basalts and Wallowa mountains uplift in northeast oregon, *Nature*, *438*, 842–845.

Hauri, E., J. Lassiter, and D. DePaolo (1996), Osmium isotope systematics of drilled lavas from Mauna Loa, Hawaii, *J. Geophys. Res.*, *101*, 11,793–11,806.

Healy, D. (2009), Short note: Elastic field in 3D due to a spheroidal inclusion-matlab® code for Eshelby's solution, *Comput. Geosci.*, *35*, 2170–2173.

Hernlund, J. W., P. J. Tackley, and D. J. Stevenson (2008), Bouyant melting instabilities beneath extending lithosphere: 1. Numerical models, *J. Geophys. Res.*, *113*, B04405, doi:10.1029/2006JB004862.

Hier-Majumder, S., S. Mei, and D. L. Kohlstedt (2005), Water weakening in clinopyroxene in diffusion creep, *J. Geophys. Res.*, *110*, B07406, doi:10.1029/2004JB003414.

Hooper, P. R., V. E. Camp, S. P. Reidel, and M. E. Ross (2007), The origin of the columbia river flood basalt province: Plume versus nonplume models, *Spec. Pap. Geol. Soc. Am.*, *430*, 635–668.

Ito, G., and P. Clift (1998), Subsidence and growth of Pacific cretaceous plateaus, *Earth Planet. Sci. Lett.*, *161*, 85–100.

Jellinek, A., and D. DePaolo (2003), A model for the origin of large silicic magma chambers: Precursors of caldera-forming eruptions, *Bull. Volcanol.*, *65*, 363–381.

Jerram, D., and M. Widdowson (2005), The anatomy of continental flood basalt provinces: Geological constraints on the processes and products of flood volcanism, *Lithos*, *79*, 385–405.

Jones, A., G. Price, N. Price, P. DeCarli, and R. Clegg (2002), Impact induced melting and the development of large igneous provinces, *Earth Planet. Sci. Lett.*, *202*, 551–561.

Jull, M., and P. Kelemen (2001), On the conditions for lower crustal convective instability, *J. Geophys. Res.*, *106*, 6423–6446.

Karato, S.-I., and H. Jung (2003), Effects of pressure on high-temperature dislocation creep in olivine, *Philos. Mag.*, *83*, 401–414.

Karlstrom, L., J. Dufek, and M. Manga (2009), Organization of volcanic plumbing through magmatic lensing by magma chambers and volcanic loads, *J. Geophys. Res.*, *114*, B10204, doi: 10.1029/2009JB006339.

Karlstrom, L., J. Dufek, and M. Manga (2010), Magma chamber stability in arc and continental crust, *J. Volcanol. Geotherm. Res.*, *190*, 249–270.

Kerrick, D. M., and G. K. Jacobs (1981), A modified Redlich-Kwong equation for H2O, CO2, and H2O-CO2 mixtures at elevated pressures and temperatures, *Am. J. Sci.*, *281*, 755–767.

King, S., and D. Anderson (1995), An alternative mechanism of flood basalt formation, *Earth Planet. Sci. Lett.*, *136*, 269–279.

Kopp, H., C. Kopp, J. Morgan, and E. Flueh (2003), Fossil hot spot-ridge interaction in the Musicians Seamount province: Geophysical investigations of hot spot volcanism at volcanic elongated ridges, *J. Geophys. Res.*, *108*(B3), 2160, doi:10.1029/2002JB002015.

Lange, R. A. (2002), Constraints on the preeruptive volatile concentrations in the columbia river flood basalts, *Geology*, *30*(2): 179–182.

Leitch, A., and G. Davies (2001), Mantle plumes and flood basalts: Enhanced melting from plume ascent and an eclogite component, *J. Geophys. Res.*, *106*, 2047–2059.

Lin, H.-C., and P. E. van Keken (2005), Multiple volcanic episodes of flood basalts caused by thermochemical mantle plumes, *Nature*, *436*, 250–252.

Lister, J., and R. Kerr (1989), The propagation of two-dimensional and axisymmetric viscous gravity currents at a fluid interface, *J. Fluid Mech.*, *203*, 215–249.

Mangan, M., T. Wright, D. Swanson, and G. Byerly (1986), Regional correlation of Grande Ronde basalt flows, Columbia River basalt group, Washington, Oregon, and Idaho, *Geol. Soc. Am. Bull.*, *97*(11), 1300–1318.

Marsh, B. (1989), On convective style and vigor in sheet-like magma chambers, *J. Petrol.*, *30*(3), 479–530.

Marzoli, A., L. Melluso, V. Morra, P. Renne, I. Sgrosso, M. D'Antonio, L. Duarte Morais, E. A. A. Morais, and G. Ricci (1999), Geochronology and petrology of cretaceous basaltic magmatism in the Kwanza basin (Western Angola), and relationships with the Parana-Etendeka continental flood basalt province, *J. Geodyn.*, *28*, 341–356.

McNutt, M., and A. Bonneville (2000), A shallow, chemical origin for the Marquesas swell, *Geochem. Geophys. Geosyst.*, *1*(6), 1014, doi:10.1029/1999GC000028.

Moon, P., and D. Spencer (1988), *Field Theory Handbook, Including Coordinate Systems, Differential Equations, and Their Solutions*, 2nd ed., Springer, New York.

Morgan, W. (1971), Convection plumes in the lower mantle, *Nature*, *230*, 42–43.

Nielsen, T., and C. Brooks (1981), The E. Greenland rifted continental-margin: An examination of the coastal flexure, *J. Geol. Soc.*, *138*, 559–568.

Norminton, E., and J. Blackwell (1964), Transient heat flow from constant temperature spheroids and the thin circular disk, *Q. J. Mech. Appl. Math.*, *17*(1), 65–72.

Papale, P. (1999), Modeling of the solubility of a two-component H2O + CO2 fluid in silicate liquids, *Am. Mineral.*, *84*, 477–492.

Parsons, T., N. H. Sleep, and G. H. Thompson (1992), Host rock rheology controls on the emplacement of tabular intrusions: Implications for underplating of extending crust, *Tectonics*, *11*(6), 1348–1356.

Ramalho, R., G. Helffrich, M. Costa, D. Vance, D. Hoffmann, and D. N. Schmidt (2010), Episodic swell growth inferred from variable uplift of the cape verde hotspot islands, *Nat. Geosci.*, *3*, 774–777.

Ray, R., H. C. Sheth, and J. Mallik (2007), Structure and emplacement of the Nandurdar-Dhule mafic dyke swarm, Deccan traps, and the tectono-magmatic evolution of flood basalts, *Bull. Volcanol.*, *69*, 537–551.

Richards, M., R. Duncan, and V. Courtillot (1989), Flood basalts and hot-spot tracks: Plume heads and tails, *Science*, *246*(4926), 103–107.

Ridley, V., and M. Richards (2010), Deep crustal structure beneath large igneous provinces and the petrologic evolution of flood basalts, *Geochem. Geophys. Geosyst.*, *11*, Q09006, doi:10.1029/2009GC002935.

Roberge, J., P. J. Wallace, R. V. White, and M. F. Coffin (2005), Anomalous uplift and subsidence of the Ontong Java plateau inferred from CO2 contents of submarine basaltic glasses, *Geology*, *33*(6), 501–504.

Rubin, A. M. (1995), Propagation of magma-filled cracks, *Annu. Rev. Earth Planet. Sci.*, *23*, 287–336.

Rybacki, E., and G. Dresen (2000), Dislocation and diffusion creep of synthetic anorthite aggregates, *J. Geophys. Res.*, *105*, 26,017-26,036.

Saunders, A., S. Jones, L. Morgan, K. Pierce, M. Widdowson, and Y. Xu (2007), Regional uplift associated with continental large igneous provinces: The roles of mantle plumes and the lithosphere, *Chem. Geol.*, *241*, 282–318.

Schmeling, H. (2006), A model of episodic melt extraction for plumes, *J. Geophys. Res.*, *111*, B03202, doi:10.1029/2004JB003423.

Sleep, N. H. (2007), Edge-modulated stagnant-lid convection and volcanic passive margins, *Geochem. Geophys. Geosyst.*, *8*, Q12004, doi:10.1029/2007GC001672.

Sleep, N. H., C. J. Ebinger, and J. M. Kendell (2002), Deflection of mantle plume material by cratonic keels, *Geol. Soc. Spec. Publ.*, *199*, 135–150.

Smyth, J. R., D. J. Frost, F. Nestola, C. M. Holl, and G. Bromiley (2006), Olivine hydration in the deep upper mantle: Effects of temperature and silica activity, *Geophys. Res. Lett.*, *33*, L15301, doi:10.1029/2006GL026194.

Storey, M., R. Duncan, and C. Tegner (2007), Timing and duration of volcanism in the north atlantic igneous province: Implications for geodynamics and links to the Iceland hotspot, *Chem. Geol.*, *241*, 264–281.

Tanton, L., and B. Hager (2000), Melt intrusion as a trigger for lithospheric foundering and the eruption of the Siberian flood basalts, *Geophys. Res. Lett.*, *27*(23), 3937–3940.

Tegner, C., C. Brooks, R. Duncan, L. Heister, and S. Bernstein (2008), ^{40}Ar-^{39}Ar ages of intrusions in East Greenland: Rift-to-drift transition over the iceland hotspot, *Lithos*, *101*, 480–500.

Traversa, P., V. Pinel, and J. R. Grasso (2010), A constant influx model for dike propagation: Implications for magma reservoir dynamics, *J. Geophys. Res.*, *115*, B01201, doi:10.1029/2009JB006559.

Watts, A., and U. T. Brink (1989), Crustal structure, flexure, and subsidence history of the Hawaiian islands, *J. Geophys. Res.*, *94*, 10,473–10,500.

White, R. S., L. K. Smith, A. W. Roberts, P. A. F. Christie, N. J. Kusznir, A. M. Roberts, D. Healy, R. Spitzer, A. Chappel, and J. D. Eccles (2008), Lower-crustal intrusion on the North Atlantic continental margin, *Nature*, *452*, 460–464.

Whittington, A., A. Hofmeister, and P. Nabelek (2009), Temperature-dependent thermal diffusivity of the Earth's crust and implications for magmatism, *Nature*, *458*, 319–321.

Wolff, J. A., F. C. Ramos, G. L. Hart, J. D. Patterson, and A. D. Brandon (2008), Columbia River flood basalts from a centralized crustal magma system, *Nat. Geosci.*, *1*, 177–180.

L. Karlstrom and M. A. Richards, Department of Earth and Planetary Science, University of California, 307 McCone Hall, Berkeley, CA 94720, USA. (leif@berkeley.edu; mark_richards@berkeley.edu)